

# communications

## earth & environment

### ARTICLE



<https://doi.org/10.1038/s43247-023-00803-8>

OPEN

## Southern California winter precipitation variability reflected in 100-year ocean salinity record

Sierra M. Byrne<sup>1</sup>✉, Mark A. Merrifield<sup>1</sup>, Melissa L. Carter<sup>1</sup>, Daniel R. Cayan<sup>1</sup>, Reinhard E. Flick<sup>1</sup>, Alexander Gershunov<sup>1</sup> & Sarah N. Giddings<sup>1</sup>

Rainfall in southern California is highly variable, with some fluctuations explainable by climate patterns. Resulting runoff and heightened streamflow from rain events introduces freshwater plumes into the coastal ocean. Here we use a 105-year daily sea surface salinity record collected at Scripps Pier in La Jolla, California to show that El Niño Southern Oscillation and Pacific Decadal Oscillation both have signatures in coastal sea surface salinity. Averaging the freshest quantile of sea surface salinity over each year's winter season provides a useful metric for connecting the coastal ocean to interannual winter rainfall variability, through the influence of freshwater plumes originating, at closest, 7.5 km north of Scripps Pier. This salinity metric has a clear relationship with dominant climate phases: negative Pacific Decadal Oscillation and La Niña conditions correspond consistently with lack of salinity anomaly/ dry winters. Fresh salinity anomalies (i.e., wet winters) occur during positive phase Pacific Decadal Oscillation and El Niño winters, although not consistently. This analysis emphasizes the strong influence that precipitation and consequent streamflow has on the coastal ocean, even in a region of overall low freshwater input, and provides an ocean-based metric for assessing decadal rainfall variability.

<sup>1</sup> Scripps Institution of Oceanography, University of California San Diego, La Jolla, CA, USA. ✉email: [s2byrne@ucsd.edu](mailto:s2byrne@ucsd.edu)

**S**outhern California precipitation, or lack thereof, occurs in extremity, resulting in multiyear droughts with sporadic years of heavy rainfall and nearly the highest year-to-year precipitation variability in the continental United States<sup>1</sup>. Owing to its lower mid-latitude setting on the eastern flank of the North Pacific High, heavy precipitation occurs relatively rarely, but can carry high intensities<sup>2–4</sup>, sometimes on par with those observed in climatologically wetter region of central California<sup>5</sup>. Climate change is projected to exacerbate this pre-existing hydroclimate volatility by reducing the frequency of low- to medium-intensity precipitation while increasing the intensity and contribution of extreme storms<sup>6</sup>. Above-average rainfall years are critical for replenishing valuable water supplies to meet growing agricultural and direct human consumption needs. Precipitation also helps to moderate wildfire risk<sup>7</sup>, a costly consequence of dry foliage and long dry periods. In 2018 alone during a severe drought year, California's wildfires cost the US an estimated \$148.5 billion<sup>8</sup>. The occurrence of extreme rain events and runoff can also have devastating effects across southern California in the form of flooding<sup>9–11</sup>, debris flow<sup>12</sup>, and contamination of coastal waters<sup>13,14</sup>.

The mean dry conditions in southern California result in local streams and rivers having little outflow during most of the year. When heavy rain events do occur, primarily during the winter season, outflow increases by orders of magnitude and plumes of freshwater propagate into the coastal ocean<sup>15</sup>. In addition, non-point source runoff delivers freshwater to coastal waters. Storm runoff is known to carry pollutants through watersheds to the ocean, reducing local water quality, increasing fecal indicator bacteria signals, and posing public health risks<sup>13,14</sup>. Runoff and river waters also carry other accumulated properties or quantities, including nutrients (important for biological productivity<sup>16,17</sup>) and sediment, important for coastal morphology and sand budgets<sup>18</sup>.

Climate indices often are used to characterize atmospheric and oceanic patterns favorable to wet or dry conditions over western North America<sup>19–21</sup>. In particular for the southern California region, El Niño Southern Oscillation (ENSO) usually brings drought-like conditions in La Niña phase and a higher probability of intense rainfall during strong El Niño years<sup>21</sup>. Other studies have considered the influence of the Pacific Decadal Oscillation (PDO) on winter rainfall in the study region<sup>22–24</sup>. Shukla et al. 2015 found that the negative PDO phase increases the probability of drought favorable conditions in southern California over the late winter months<sup>24</sup>. PDO modulates ENSO teleconnections, including precipitation<sup>25</sup>, and contributes to seasonal precipitation prediction skill in the study region<sup>26</sup>. Negative PDO and ENSO phases have been linked to increased fire activity in the southwestern US due to decreased precipitation<sup>27</sup>. These climate phases impact the hydrology in the study region due to the latitudinal shifts in the atmospheric pressure systems that are precipitation-bearing versus precipitation-blocking<sup>21</sup>.

In this study, we utilize sea surface salinity data to investigate precipitation and climate variability. Over a century of daily sea surface salinity measurements have been recorded at the Scripps Institution of Oceanography Pier. The standardized collection procedures<sup>28</sup> provide confidence that the salinity measurements are consistent over time. This long record enables a unique 105-year investigation of hydroclimate variation affecting the Southern California coastal region. Annual-averages of the pier salinity record have been used to assess wind-driven upwelling<sup>29</sup>, but freshwater spikes in the daily record have not been well characterized. In this paper, we demonstrate the potential for using coastal salinity to infer runoff from heavy rain events over the wet winter season when fresh salinity spikes are most prevalent. Here we use a 105-year daily sea surface salinity record to show that El

Niño Southern Oscillation and Pacific Decadal Oscillation both have signatures in coastal sea surface salinity even in a region which receives small total freshwater input (through either direct precipitation or runoff). Specifically, we find that the freshest salinity quantile is a good indicator of year-to-year variations in precipitation and runoff, highlighting the connection between the coastal ocean and the influence of storm activity, or lack thereof, in correspondence with known climate phase shifts.

## Results and discussion

**Precipitation influence on surface salinity.** The daily SSS record from Scripps Pier (Fig. 1a) exhibits spike-like fresh events ranging from  $-5.6$  to  $-0.3$  psu (Practical Salinity Unit), contributing to a negative skewness ( $-2.84$ ) about a mean value of  $33.58$  psu. A blowup of the record during January through March (JFM) for one year (2003 typifies average conditions) shows that the fresh SSS spikes align with winter rain events that last for 1–5 days (Fig. 1b). Within 1–3 days following each rain peak, salinity at the pier drops abruptly by several tenths psu, and slowly returns to near pre-event values after several weeks. Local streamflow exhibit a near identical pattern to that of the precipitation over the events, with the streamflow peaking within a day of the maximum rainfall (Fig. 1b). The SSS, precipitation, and streamflow measurements are recorded at locations within 20 km of each other (see map in Supplementary Fig. 1). To quantify this relationship over the longer record, we composite JFM SSS relative to streamflow anomalies, which confirms that, on average, SSS drops for weeks following sizeable outflow events (Fig. 2). Compounding effects lead to variations in the timing and amplitude of the SSS response relative to a given streamflow or precipitation level. This is evident in the 2003 record (Fig. 1b) as the largest rain event does not result in the lowest SSS response, but this largest SSS response is the third event in  $\sim 1$  month span.

Numerous factors influence ocean salinity in the study region. Coastal upwelling increases SSS by vertical transport of deep cold salty water to the surface and peaks in the April–July summer period<sup>30</sup>. Therefore, this work focusing on winter freshwater events does not investigate upwelling-induced changes. During rain events, atmospheric freshwater input lowers the salinity of the coastal ocean. An additional factor that directly alters surface salinity is horizontal advection. It is unspecified in existing literature whether offshore water mass advection variability influences the nearshore surface waters of the study region. The SSS drops seen at Scripps Pier are sudden and extreme, consistently corresponding in time with rain and streamflow spikes (Figs. 1b and 2). This suggests that the most practical mechanisms for these SSS drops are from precipitation directly, localized runoff during extreme events, and the precipitation-driven streamflow increases and resulting freshwater plumes that propagate into the coastal ocean. The connection between winter rain events and the SSS and hydrology of the nearshore coastal zone in the region has not been examined to our knowledge on yearly to interdecadal time scales and will be a focus of this study. Interannual streamflow variability in larger river systems due to precipitation has been shown to change coastal ocean dynamics<sup>31,32</sup>. Our work shows that even small, intermittent freshwater plumes have a robust impact on coastal ocean freshening in the study region.

River plumes of this relatively fresh stormwater infiltrate the salty ocean waters with a plume area dependent on the amount of rainfall<sup>33</sup>. The fate of the plume depends on the relative strength of the discharge and the waves. Plumes during relatively small discharge and large waves are trapped in the surfzone and travel along the coast in the direction of the surfzone wave-driven currents<sup>34–36</sup>, whereas intermediate to large discharge can escape

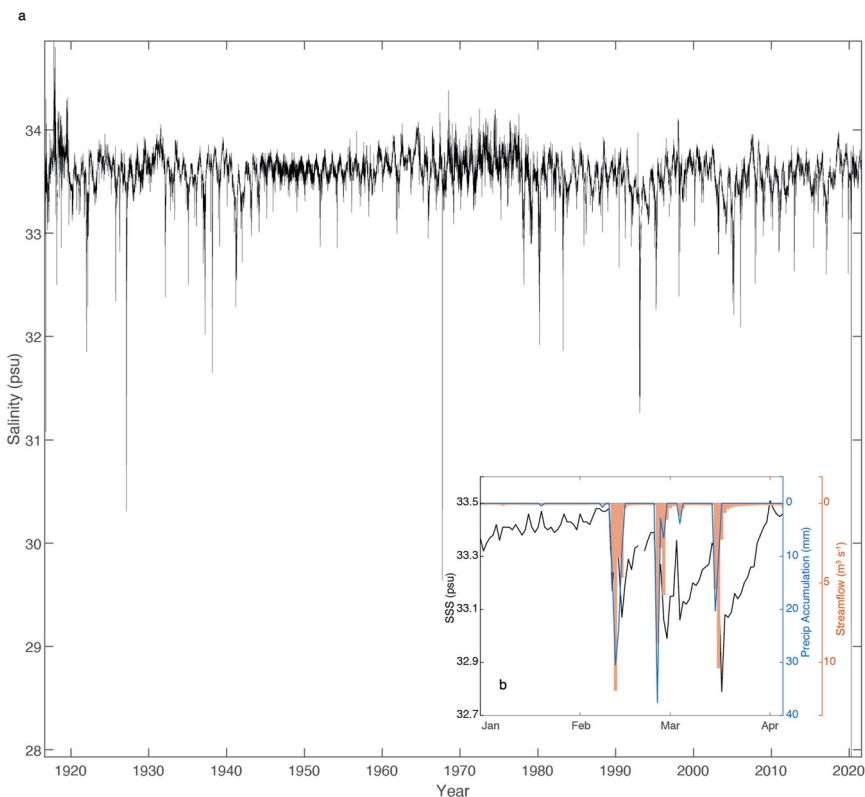


**Fig. 1 Time series of local sea surface salinity, precipitation, and streamflow.** **a** Daily sea surface salinity (SSS) measurements from surface water samples at the Scripps Pier, spanning 1916–2021. **b** The correspondence between daily SSS (black), San Diego Airport daily rainfall (blue, inverted y-axis), and Los Peñasquitos daily streamflow (orange bars, inverted y-axis) is illustrated for January–March of 2003 to highlight a typical winter season.

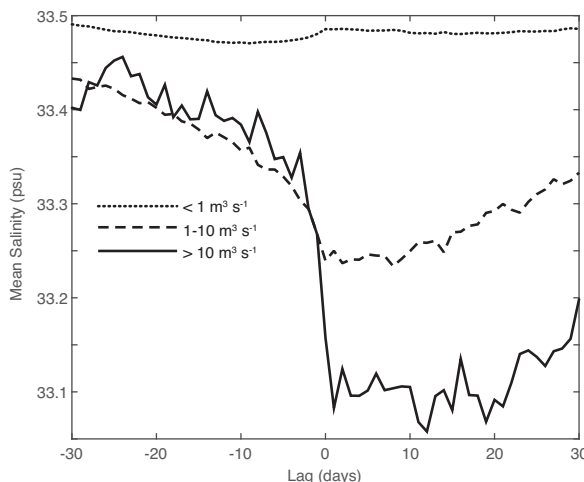


**Fig. 2 Sea surface salinity preceding and following streamflow events of three magnitudes.** Sea surface salinity data shown 30 days prior and 30 days following Los Peñasquitos streamflow events of three categories, low flow  $<1 \text{ m}^3 \text{ s}^{-1}$  (dotted line), medium flow  $1-10 \text{ m}^3 \text{ s}^{-1}$  (dashed line), and high flow  $>10 \text{ m}^3 \text{ s}^{-1}$  (solid black line).

the surfzone and travel along the coast depending upon the inner-shelf currents<sup>37,38</sup>. The direction plumes travel in the inner-shelf varies with wind speed and direction, river discharge inertia, and buoyancy<sup>15</sup>. River plumes over the shelf in southern California frequently travel southward along the coast due to the relative timing of regional precipitation and wind patterns<sup>15</sup>, which has implications for the study site located 7.5 km south of the Los Peñasquitos Lagoon and 12 km south of the San Dieguito River

(see map in Supplementary Fig. 1). The interaction of freshwater discharge plumes with the surfzone and nearshore is a topic of active research. The SSS time delay relative to the peak rain/streamflow event suggests that the southward advection of local river plumes/estuary outflows contribute to the Scripps signal<sup>15</sup>. In addition, the SSS decay time likely reflects advective-diffusive time scales of the plume.

The fresh salinity events at Scripps Pier can occur throughout the year but are most prevalent during JFM, the three freshest months on average (Fig. 3). The JFM winter season also corresponds to seasonal highs in Los Peñasquitos streamflow and San Diego Airport rainfall. Approximately half the annual rainfall in the San Diego Airport record occurs during JFM, consistent with estimates for the larger San Diego region (Hydroclimate Report Water Year 2016, <https://water.ca.gov>). We focus the remainder of our analyses on the JFM winter season of high rainfall, highest streamflow, and lowest salinity (Fig. 3).

To represent the freshest winter salinity values, the 10% quantile of the JFM salinity anomaly (hereinafter referred to as  $\text{SSS}_{10}$ ) is computed each year after removing the JFM average for that year to de-emphasize background oceanic variability. Similar salinity values to  $\text{SSS}_{10}$  are obtained by subtracting the median quantile from the 10% quantile for each JFM season. The 10% quantile of the remaining anomaly array is the selected metric as it isolates the most extreme negative values for each year (see Supplementary Fig. 2 for explanation of quantile calculations).

The  $\text{SSS}_{10}$  time series captures year-to-year freshening in the JFM winter season. In years of low precipitation,  $\text{SSS}_{10}$  (Fig. 4a) remains relatively consistent at a near zero anomaly (0 to  $-0.2 \text{ psu}$ ). The strong correlations of  $\text{SSS}_{10}$  to precipitation and streamflow (Supplementary Fig. 2) further confirm that the 10% anomalous quantile characterizes the local response of SSS to

rainfall. As a check on the representativeness and reliability of the Scripps SSS<sub>10</sub> time series, we compare it to a similar estimate of the 10% quantile from the Newport Pier SSS measurements (Supplementary Fig. 3). A strong significant ( $p < 0.05$ ) correspondence between the SSS<sub>10</sub> time series of Scripps and Newport ( $r = 0.74$ ) suggests that the rain-related coastal SSS signal is widespread (i.e., not just representative at this one location) and

robust in the daily pier measurements (i.e., not subject to changes in observers or methodology).

Together the SSS<sub>10</sub>, streamflow, and precipitation series highlight especially wet winters ( $SSS_{10} < -0.35$ ) against a background of otherwise dry conditions (Fig. 4a, b). The SSS<sub>10</sub> record particularly emphasizes consecutive dry years during predominantly negative PDO phases (Fig. 4a, c). A noteworthy feature in the SSS<sub>10</sub> record is the negative PDO phase of 1944–1977 (Fig. 4c) when the precipitation and streamflow are weak and the SSS<sub>10</sub> is nearly constant for 30+ years. During the two extended negative PDO phases, with the exception of 2005, the JFM-averaged precipitation anomaly remains under 40 mm. In addition, multi-year droughts in excess of 3 years appear to be less apparent in the first 25 years of the SSS<sub>10</sub> record, prior to the 30-year long dry period. While dry winters tend to occur sequentially, one low SSS/wet winter is rarely followed by another. A potential source of this shorter-term variability in SSS<sub>10</sub>/precipitation is ENSO phase (Fig. 4d).

High, significant correlations between SSS<sub>10</sub> and the JFM precipitation accumulation anomaly ( $r = -0.78$ ) and Los Peñasquitos streamflow anomaly ( $r = -0.83$ ) further support that SSS<sub>10</sub> reflects rainfall and runoff variability (Fig. 4a, b). High correlations of SSS<sub>10</sub> to regional precipitation (Fig. 5) and streamflow suggest SSS<sub>10</sub> captures freshwater drainage of the greater coastal watershed (see watershed in Supplementary Fig. 1). The SSS signal tracks more closely with streamflow than with precipitation because of the delay in advection of streamflow to the coastal ocean. The probability of below average JFM daily streamflow is highest in the “saltiest” years ( $SSS_{10} > -0.2$  psu) and lowest in the “freshest” years ( $SSS_{10} < -0.35$  psu; Supplementary Fig. 4).

The tails of the daily streamflow distributions (Supplementary Fig. 4) highlight differences in the number of large outflow events during fresh, moderately fresh, and salty years. In salty years, the probability of rain events causing sustained high streamflow is much lower than that of the freshest years. The fresh years that

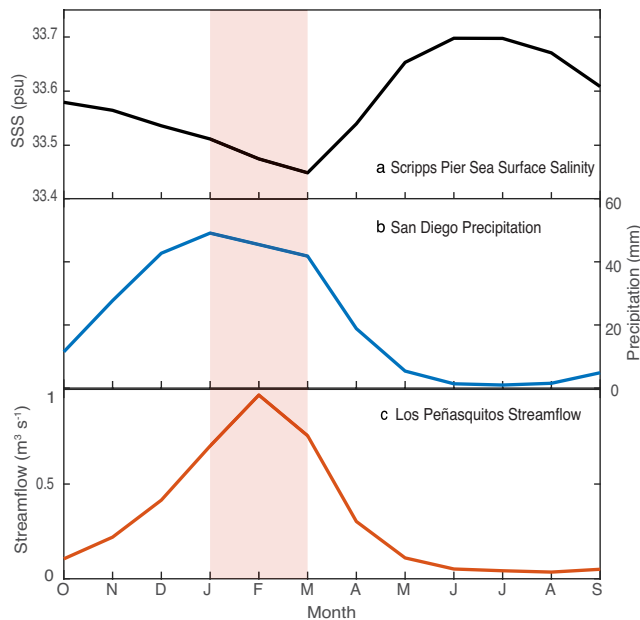


**Fig. 3 Seasonal cycles of sea surface salinity, precipitation, and streamflow.** Average monthly values of **a** SSS, **b** accumulated precipitation at San Diego Airport (NOAA NCEI), and **c** Los Peñasquitos streamflow (USGS). The red band highlights the wet winter JFM season.

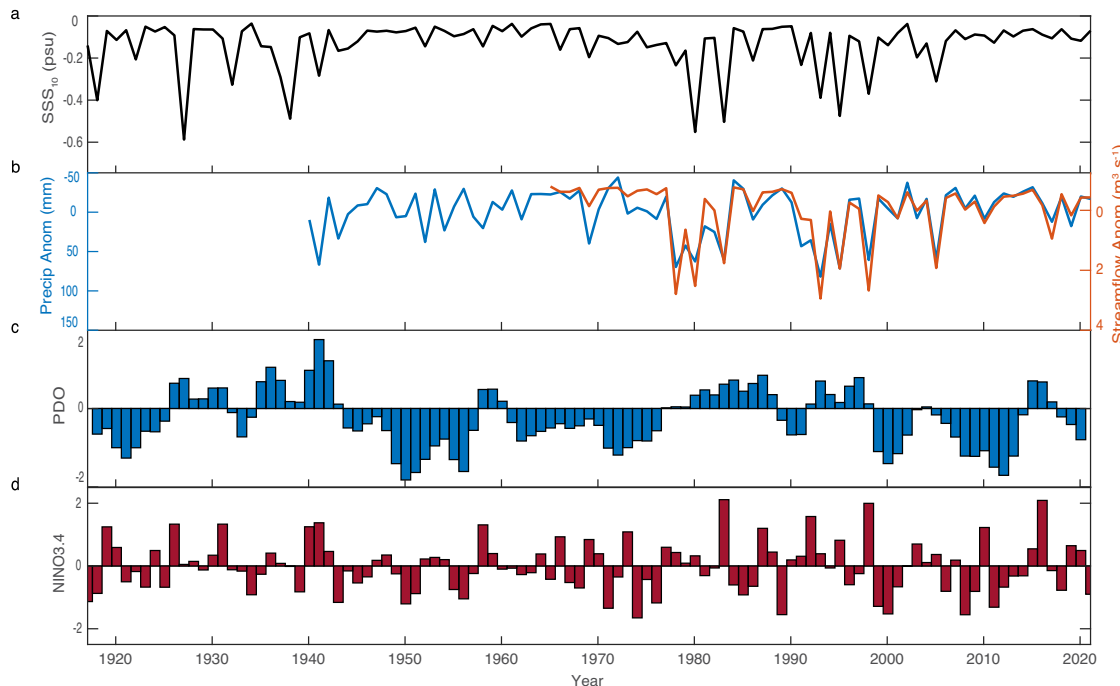


**Fig. 4 The SSS<sub>10</sub> metric presented alongside winter precipitation and streamflow anomalies and relevant climate indices. **a** SSS<sub>10</sub> (1917–2021). **b** JFM-averaged precipitation (blue, 1940–2021) and streamflow (orange, 1965–2021) anomalies with climatological monthly averages removed, shown with flipped y-axes. **c** 5-year smoothed JFM-averaged PDO index values. **d** JFM-averaged NINO3.4 index values.**

feature the largest  $SSS_{10}$  anomalies (Fig. 4a) correspond to generally higher chances of sustained intense streamflow (Supplementary Fig. 4). The distribution of streamflow highlights that heavy rain events occur less frequently in salty/dry years than fresh years.

To further explore the connection between Scripps Pier salinity and regional winter precipitation patterns, we examine correlations between  $SSS_{10}$  and the Livneh gridded precipitation product<sup>39</sup> for 1917–2011. JFM-averaged precipitation exhibits statistically significant correlations ( $|r| > 0.20$ ) with  $SSS_{10}$  over a broad swath of the southwestern US, with the highest correlations (up to  $r = -0.79$ ) in the Southern California region (Fig. 5). The low  $SSS_{10}$ /high rain winters appear to be indicative of large-scale precipitation patterns that affect a large part of the Southwest region.

**Surface salinity and climate modes.** We next consider the extent to which Pacific climate modes can provide context and a degree of predictability for the JFM precipitation and runoff captured by the  $SSS_{10}$  time series. For comparison with  $SSS_{10}$ , the NINO3.4 and PDO indices are JFM-averaged. The strongest ENSO teleconnections, linking the tropical and midlatitude conditions, occur in JFM<sup>40</sup>. Correlations between  $SSS_{10}$  and PDO and ENSO indices are weak with  $r = -0.28$  ( $p = 0.24$ ), and  $r = -0.25$  ( $p = 0.01$ ), respectively. Despite the low correlation with the

PDO, multi-year periods of high  $SSS_{10}$ /low rain generally correspond to negative PDO phases (Fig. 4a, c).

Scatter plots confirm that while the linear correlations between  $SSS_{10}$  and indices of the PDO (Fig. 6a) and ENSO (Fig. 6b) are weak, there is a strong tendency for high  $SSS_{10}$ /low rain winter seasons during negative values of both indices<sup>23–26</sup>. The case for the PDO is slightly less obvious for annual values, but with a 5-year smoothing to emphasize decadal polarity changes, the relationship is tighter (Fig. 6a).

JFM ENSO state provides a stronger constraint on year-to-year drought conditions than the PDO, with only one low  $SSS_{10}$  winter (in 1918) evident when the ENSO index dips below  $-0.2$ , and none during strong La Niña events when the JFM-averaged index falls below  $-1.0$  (Fig. 6b). Thus, La Niña-like conditions strongly favor below-average rain levels for any given winter<sup>25</sup>, whereas multi-year drought periods tend to fall within prolonged negative PDO phases. In contrast, wet winters occur during positive PDO and ENSO phases<sup>25</sup>, but not consistently so as high  $SSS_{10}$ /dry winters are just as likely, and high index values do not ensure low  $SSS_{10}$  levels (Fig. 6a, b). The wettest/lowest  $SSS_{10}$  winters almost exclusively occur during El Niño years, but not every El Niño resulted in a wet year. Low  $SSS_{10}$ /wet winters ( $SSS_{10} < -0.35$ ) occurred during 17.1% (12.8%) of positive PDO (El Niño) years, but only 1.6% (3.5%) of negative PDO (La Niña) winters. High  $SSS_{10}$ /dry winters ( $SSS_{10} > -0.20$ ) happened in 73.2% (76.6%) of positive PDO (El Niño) years and in 91.9% (91.4%) of negative PDO (La Niña) winters.

A recent study<sup>41</sup> notes that the Tropical Northern Hemisphere pattern<sup>42</sup> (TNH) is highly correlated with California precipitation variability, and suggests that a combination of ENSO and TNH indices (as opposed to ENSO alone) provides improved predictability of precipitation. TNH is a prominent winter climate mode that reflects large-scale changes in the extent and location of the Pacific jet stream<sup>42</sup>. Dry/wet years in southern California tend to occur during TNH positive/negative phases. A strong negative 500-hPa geopotential height anomaly is seen at TNH negative phases over the NE Pacific Ocean, and vice versa for positive phases<sup>43</sup>. Negative phase TNH conditions support cloud formation and precipitation whereas positive phase TNH conditions reduce the winter storm landfalling probability in California<sup>41</sup>. A scatter plot of  $SSS_{10}$  versus the NINO3.4 and TNH indices confirms these tendencies, with low  $SSS_{10}$  wet winters clustered primarily in the lower right-hand quadrant of Fig. 6c where El Niño and negative TNH conditions meet.

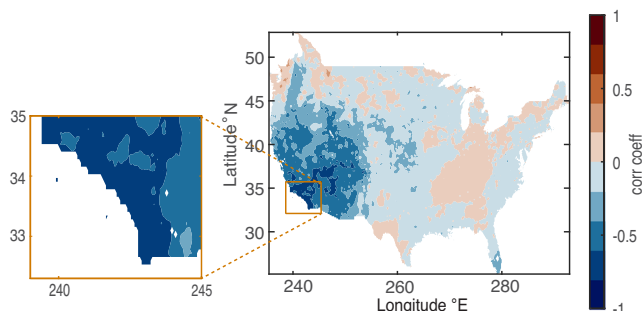


**Fig. 5 Correlation of the  $SSS_{10}$  metric with US precipitation.** Correlation coefficient contour map of  $SSS_{10}$  to Livneh gridded precipitation<sup>39</sup> (1917–2011). Inset on the left shows southern California north of the US–Mexico border and south of San Luis Obispo. Colormap from ref. <sup>54</sup>.

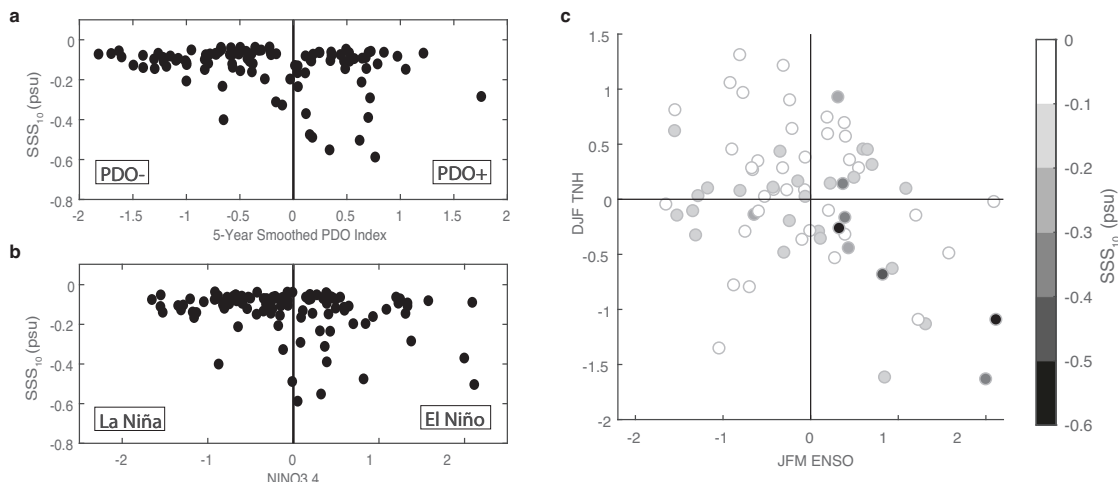


**Fig. 6 Division of  $SSS_{10}$  by relevant climate indices.** Scatter of  $SSS_{10}$  (1917–2021) versus **a** 5-year smoothed JFM-averaged PDO index and **b** JFM-averaged NINO3.4 index. **c** Scatter of JFM-averaged NINO3.4 index with DJF-averaged TNH index, colored by the corresponding  $SSS_{10}$  for each year (1951–2021).

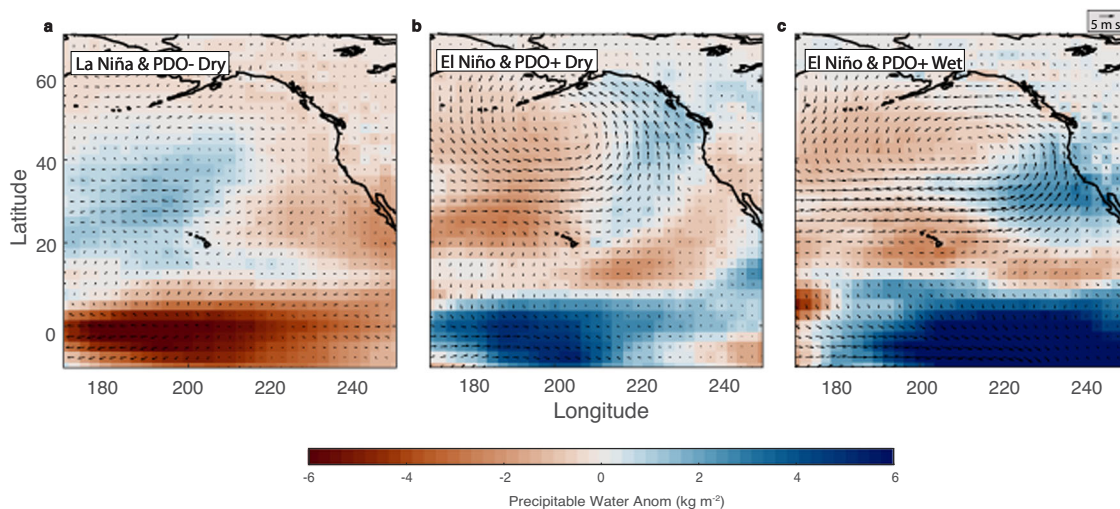


**Fig. 7 Composite atmospheric conditions for three combinations of climate modes and  $SSS_{10}$  wet vs. dry winter groupings.** Composites of JFM-averaged anomalies of NCEP surface winds and precipitable water (1981–2021) for **a** La Niña & PDO negative phases with high  $SSS_{10}$ /dry winters ( $n = 13$  yrs), **b** El Niño & PDO positive phases with high  $SSS_{10}$ /dry winters ( $n = 6$  yrs), and **c** El Niño & PDO positive phases with low  $SSS_{10}$ /wet winters ( $n = 4$  yrs). Colormap from ref. <sup>54</sup>.

Composites of JFM-averaged surface wind and precipitable water anomalies illustrate the relationship between climate phase and southern California precipitation. During La Niña and negative PDO phases (Fig. 7a), the Aleutian low pressure system over the northeast Pacific weakens (clockwise wind anomaly) with negative precipitable water anomalies and average wind conditions over the western US. During El Niño and positive PDO phase wet years (Fig. 7c), the Aleutian low strengthens and deepens (anticlockwise wind anomaly) forcing the Northern Hemisphere Jetstream (NHJ) southward, resulting in increased storm landfalls on the US west coast and significant positive precipitable water anomalies<sup>44,45</sup>. During El Niño and positive PDO phase dry years (Fig. 7b), the southeastern extent of the NHJ is located more northwest when compared to rainy year conditions (Fig. 7c), pushing storm landfalls north and causing negligible to negative precipitable water anomalies in the southern California region.

**Implications.** The long-running salinity record from Scripps Pier reflects regional winter precipitation and streamflow patterns influenced by both the PDO and ENSO. Over the past 70 years, the majority of low  $SSS_{10}$ /wet winters have occurred during positive PDO phases, and more specifically when the NINO3.4 and TNH indices are positive and negative, respectively. The  $SSS_{10}$  time series especially highlights the occurrences of multi-year drought conditions over the past century. In particular, during the prolonged negative PDO phase between 1944 and 1977,  $SSS_{10}$  was persistently near normal (Fig. 4b), indicating a lack of heavy winter rain events.

The  $SSS_{10}$  observations suggest that a freshwater signal in the coastal surface ocean that persists for multiple days requires a major rain event or a few smaller rain events that result in substantial streamflow and runoff when averaged over the JFM season. Large impact rain events can come in the form of atmospheric rivers (ARs). AR events in the southern California region occur over a few days each year and can contribute up to half of the annual precipitation accumulation<sup>46</sup>. Based on the AR Rank database, the 1978 to 1999 positive PDO phase featured 50% more days with winter AR events in the southern California region compared to the 1944–1977 negative PDO phase ( $12 \pm 1.3\%$  (twice standard error) to  $8 \pm 1.1\%$  respectively). AR

events previously have been shown to contribute more to the total water year precipitation during PDO+ and El Niño years in southern California<sup>1,46</sup> when compared to other years. In general, we find that mean JFM precipitation provides a better correspondence with  $SSS_{10}$  than time series based on AR Rank, as expected, due to ARs providing only some of the precipitation to the region. This implies that not all ARs lead to wet winters, as measured by the coastal ocean's SSS response, and the sources of precipitation that lead to low  $SSS_{10}$  winters are variable.

As the climate changes, current projections are uncertain regarding how the climate modes influencing the southern California region will be impacted<sup>47</sup>. The IPCC WGII Sixth Assessment Report<sup>47</sup> states with moderate confidence that extreme El Niño and La Niña events may become more frequent, up to twice as often, with increased teleconnection responses over the remainder of this century. This would have a direct impact on the severity of dry winters and of the unpredictable wet winters in southern California. A consensus on future PDO conditions under climate change has not been reached<sup>47</sup>. The US west coast may experience a decrease in the frequency of non-AR related rain but an increase in extreme rain due to ARs specifically<sup>6</sup>.

The ocean salinity time series at Scripps Pier complements information provided by nearby streamflow data and reinforces the detection of interannual and decadal winter rainfall variations apparent in rain gauge data. The salinity record also provides a long-term context for assessing the impacts of extreme precipitation events on the coastal zone, even in a region of low total freshwater input, which has impacts on coastal pollution, sediment, nutrient delivery, and beyond. Results here provide a more nuanced view of the value of the coastal salinity record, in that event scale structure in the form of low SSS pulses (or lack of these) provides a gauge of the vital heavy precipitation events that dictate the status of precipitation and water resources in the southern California coastal region. Together the measurements highlight the strong influence that Pacific climate modes have on regional precipitation and coastal hydrography. The 105-year length of this salinity record provides a unique opportunity to isolate these decadal patterns in precipitation as it scales with the coastal ocean response to these events. Our findings show that salinity can be used to investigate the strong role that interannual to multi-decadal variation plays in driving hydroclimate conditions in this region – multi-decadal periods of relatively dry

winters are common for the region and relief from drought periods may not occur until the PDO shifts to a positive state. From revealing climate signals not shown in salinity data previously, to bolstering proof that precipitation and resulting advection of streamflow waters are the leading causes in coastal ocean freshening events, the implications for this study increase the breadth of surface salinity records beyond the uses by oceanographers alone.

## Methods and data

**Salinity data.** Since 1916, daily water samples have been collected at the end of the Scripps Institution of Oceanography (SIO) pier in La Jolla, CA. For the near-surface samples, salinity has been measured with two consistent methodologies over time, initially by titration (1916–1964) and now by inductive salinometer (1965–present). The current collection and measurement procedures are described in the Shore Stations Program Annual Reports (<https://shorestations.ucsd.edu/>). Here we analyze the year-to-year wet season variability using the daily sea surface salinity (SSS) record spanning 1916 to 2021 for a total of 38,330 days of data. We also examine similar daily salinity measurements collected at the Newport Beach Pier following the same methodology. Time series from both stations are part of the Shore Stations Program<sup>28</sup>.

**Precipitation and streamflow.** Daily and monthly precipitation accumulation data (1939–2021) for the San Diego International Airport (~16 km southeast of the Pier) were obtained from the National Oceanic and Atmospheric Administration's National Center for Environmental Information (NOAA NCEI). The Livneh daily near-surface gridded precipitation data<sup>39</sup> (1915–2011) spans the continental US in 1/16 degree resolution and is provided by the Physical Sciences Laboratory (PSL), NOAA.

Daily streamflow time series from Los Peñasquitos, the closest major stream to Scripps Pier, is obtained from the U.S. Geological Survey (1965–2021). The stream feeds into Los Peñasquitos Lagoon, which discharges into the ocean ~7.5 km north of the Scripps pier. Anomalies for Los Peñasquitos outflow and monthly precipitation accumulation are the JFM averages with JFM mean climatologies removed.

An Atmospheric River rank system categorizes the magnitude of landfalling ARs based on the maximum instantaneous vertically integrated water vapor transport (IVT) and storm duration<sup>48</sup>. This work utilizes a retrospective analysis project produced daily AR Rank dataset (1948–2020) for consideration of JFM AR events<sup>46</sup>.

**Climate indices and atmospheric variables.** El Niño–Southern Oscillation (ENSO) variability is characterized using the NINO3.4 SST index (1870 to present), obtained from the PSL, NOAA. NINO3.4 is calculated from the HadISST1's SST averaged between 5°S–5°N and 170–120°W (ref. <sup>49</sup>).

The Pacific Decadal Oscillation index (1854 to present), obtained from NOAA NCEI, is computed using the ERSST Version 5 extended reconstruction of sea surface temperature<sup>50</sup>. The PDO index is smoothed using a convolution filter with a 5-year Blackman window<sup>51</sup> to emphasize decadal variability.

The Tropical/ Northern Hemisphere pattern<sup>42</sup> (TNH, 1950 to present) index was provided by the NOAA NCEP Climate Prediction Center (CPC) and accessed through Columbia University International Research for Climate and Society Institute's Climate Data Library. The TNH index is provided by the CPC with only December through February values.

For atmospheric composites (Fig. 7), surface wind (1948 to present) and precipitable water data (1981 to present) were obtained from NCEP/ NCAR Reanalysis 1 (ref. <sup>52</sup>) and NCEP Daily Global Analyses, respectively. NOAA PSL provided access to both NCEP datasets. Precipitable water content over a given area denotes humidity, which is positively correlated to rainfall<sup>53</sup>.

All climate indices are averaged over the rainy season (JFM), with the exception of TNH which is DJF averaged, and all are referred to without mention of this averaging for the sake of brevity. For all correlations, significance is determined by a *p*-value < 0.05, assuming every data point is independent unless otherwise specified.

## Data availability

The Shore Stations Program salinity data is accessible at doi.org/10.6075/J06T0K0M for the La Jolla station, and doi.org/10.6075/J0GX4BCP for the Newport Beach station. Precipitation data from NOAA NCEI is accessible at <https://www.ncdc.noaa.gov/cdo-web/datasets/GHCND/stations/GHCND-USW00023188/detail>. Livneh gridded precipitation data is accessible at <https://psl.noaa.gov/thredds/catalog/Datasets/livneh/metvars/catalog.html>. Streamflow data for Los Peñasquitos is accessible at <https://waterdata.usgs.gov/monitoring-location/11023340/>. AR rank data is accessible at <https://weclima.ucsd.edu/data-products/> and published in ref. <sup>46</sup>. NINO3.4 is accessible at <https://psl.noaa.gov/data/timeseries/monthly/NINO34/>. The PDO index is accessible at <https://www.ncei.noaa.gov/pub/data/cmb/ersst/v5/index/ersst.v5.pdo.dat>. The TNH index is accessible at <https://iridl.ldeo.columbia.edu/SOURCES/NOAA/NCEP/CPC/Indices/NHTI/TNH/datafiles.html>. Surface wind and precipitable water data from NCEP/ NCAR Reanalysis 1 and NCEP Daily Global Analyses are accessible at <https://psl.noaa.gov/thredds/catalog/Datasets/ncep.reanalysis/Dailies/surface/catalog.html>.

## Code availability

The code used in this study is available upon request to the corresponding author.

Received: 29 June 2022; Accepted: 12 April 2023;

Published online: 27 April 2023

## References

1. Dettinger, M. D., Ralph, F. M., Das, T., Neiman, P. J. & Cayan, D. R. Atmospheric rivers, floods and the water resources of California. *Water* **3**, 445–478 (2011).
2. Beighley, R. E., Melack, J. M. & Dunne, T. Impacts of California's climatic regimes and coastal land use change on stream flow characteristics. *J. Am Water Resourc. Assoc.* **39**, 1419–1433 (2003).
3. Modrick, T. M. & Georgakakos, K. P. The character and causes of flash flood occurrence changes in mountainous small basins of Southern California under projected climatic change. *J. Hydrol.: Reg. Stud.* **3**, 312–336 (2015).
4. Cannon, F. et al. Observations and predictability of a high-impact narrow cold-frontal rainband over Southern California on 2 February 2019. *Wea. Forecasting* **35**, 2083–2097 (2020).
5. Oakley, N. et al. A 22-year climatology of cool season hourly precipitation thresholds conducive to shallow landslides in California. *Earth Interactions* **22**, 1–17 (2018).
6. Gershunov, A. et al. Precipitation regime change in Western North America: the role of atmospheric rivers. *Sci. Rep.* **9**, 1–11 (2019).
7. Cayan, D. R. et al. Autumn precipitation – the competition with Santa Ana winds in determining fire outcomes in Southern California. *Int. J. Wildland Fire* **31**, 1056–1067 (2022).
8. Wang, D. et al. Economic footprint of California wildfires in 2018. *Nat. Sustain.* **4**, 252–260 (2021).
9. Corringham, T. W., Ralph, F. M., Gershunov, A., Cayan, D. R. & Talbot, C. A. Atmospheric rivers drive flood damages in the western United States. *Sci. Adv.* **5**, eaax4631 (2019).
10. Jennings, P. C. & Brooks, N. H. *Storms, Floods, and Debris Flows in Southern California and Arizona, 1978 and 1980: Proceedings of a Symposium, September 17–18, 1980*. (National Research Council, 1982).
11. Liu, T., McGuire, L. A., Oakley, N. & Cannon, F. Temporal changes in rainfall intensity–duration thresholds for post-wildfire flash floods in southern California. *Nat. Hazards Earth Syst. Sci.* **22**, 361–376 (2022).
12. Campbell, R. H. Debris flows originating from soil slips during rainstorms in Southern California. *Quart. J. Eng. Geol.* **7**, 339–349 (1974).

13. Reeves, R. L. et al. Scaling and management of fecal indicator bacteria in runoff from a coastal urban watershed in southern California. *Environ. Sci. Technol.* **38**, 2637–2648 (2004).
14. Aguilera, R., Gershunov, A. & Benmarhnia, T. Atmospheric rivers impact California's coastal water quality via extreme precipitation. *Sci. Total Environ.* **671**, 488–494 (2019).
15. Warrick, J. A. et al. River plume patterns and dynamics within the Southern California Bight. *Continental Shelf Res.* **27**, 2427–2448 (2007).
16. Howard, M. D. A. et al. Anthropogenic nutrient sources rival natural sources on small scales in the coastal waters of the Southern California Bight. *Limnol. Oceanogr.* **59**, 285–297 (2014).
17. Anderson, D. M., Glibert, P. M. & Burkholder, J. M. Harmful algal blooms and eutrophication: nutrient sources, composition, and consequences. *Estuaries* **25**, 704–726 (2002).
18. Syvitski, J. P. M. & Milliman, J. D. Geology, geography, and humans battle for dominance over the delivery of fluvial sediment to the coastal ocean. *J. Geol.* **115**, 1–19 (2007).
19. Ropelewski, C. F. & Halpert, M. S. North American precipitation and temperature patterns associated with the El Niño/Southern Oscillation (ENSO). *Mon. Wea. Rev.* **114**, 2352–2362 (1986).
20. Gershunov, A. & Barnett, T. P. ENSO influence on intraseasonal extreme rainfall and temperature frequencies in the contiguous United States: observations and model results. *J. Clim.* **11**, 1575–1586 (1998).
21. Cayan, D. R., Redmond, K. T. & Riddle, L. G. ENSO and hydrologic extremes in the western United States. *J. Clim.* **12**, 2881–2893 (1999).
22. Mantua, N. J., Hare, S. R., Zhang, Y., Wallace, J. M. & Francis, R. C. A Pacific interdecadal climate oscillation with impacts on salmon production. *Bull. Am. Meteorol. Soc.* **78**, 1069–1080 (1997).
23. Cayan, D. R., Dettinger, M. D., Diaz, H. F. & Graham, N. E. Decadal variability of precipitation over western North America. *J. Clim.* **11**, 3148–3166 (1998).
24. Shukla, S., Steinemann, A., Iacobellis, S. F. & Cayan, D. R. Annual drought in California: association with monthly precipitation and climate phases. *J. Appl. Meteorol. Climatol.* **54**, 2273–2281 (2015).
25. Gershunov, A. & Barnett, T. P. Interdecadal modulation of ENSO teleconnections. *Bull. Am. Meteorol. Soc.* **79**, 2715–2726 (1998).
26. Gershunov, A. & Cayan, D. R. Heavy daily precipitation frequency over the contiguous United States: sources of climatic variability and seasonal predictability. *J. Clim.* **16**, 2752–2765 (2003).
27. Westerling, A. L. & Swetnam, T. W. Interannual to decadal drought and wildfire in the western United States. *EOS, Trans. Am. Geophys. Union* **84**, 545–555 (2003).
28. Carter, M. L. et al. Shore Stations Program - La Jolla, Scripps Pier. In shore stations program data archive: current and historical Coastal ocean temperature and salinity measurements from California stations. *UC San Diego Library Digital Collections* <https://doi.org/10.6075/J067OK0M> (2022).
29. Di Lorenzo, E. et al. North Pacific Gyre Oscillation links ocean climate and ecosystem change. *Geophys. Res. Lett.* **35**, L08607 (2008).
30. Schwing, F. B. & Mendelsohn, R. Increased coastal upwelling in the California current system. *J. Geophys. Res. Oceans* **102**, 3421–3438 (1997).
31. Durocher, M., Requena, A. I., Burn, D. H. & Pellerin, J. Analysis of trends in annual streamflow to the Arctic Ocean. *Hydrol. Processes* **33**, 1143–1151 (2019).
32. Déry, S. J. & Wood, E. F. Decreasing river discharge in northern Canada. *Geophys. Res. Lett.* **32**, L10401 (2005).
33. Nezlin, N. P., DiGiacomo, P. M., Stein, E. D. & Ackerman, D. Stormwater runoff plumes observed by SeaWiFS radiometer in the Southern California Bight. *Remote Sens. Environ.* **98**, 494–510 (2005).
34. Wong, S. H., Monismith, S. G. & Boehm, A. B. Simple estimate of entrainment rate of pollutants from a coastal discharge into the surf zone. *Environ. Sci. Technol.* **47**, 11554–11561 (2013).
35. Rodriguez, A. R., Giddings, S. N. & Kumar, N. Impacts of nearshore wave-current interaction on transport and mixing of small-scale buoyant plumes. *Geophys. Res. Lett.* **45**, 8379–8389 (2018).
36. Kastner, S. E., Horner-Devine, A. R. & Thomson, J. M. A conceptual model of a river plume in the surf zone. *J. Geophys. Res. Oceans* **124**, 8060–8078 (2019).
37. Grimes, D. J., Feddersen, F., Giddings, S. N. & Pawlak, G. Cross-shore deformation of a surfzone-released dye plume by an internal tide on the inner shelf. *J. Phys. Oceanogr.* **50**, 35–54 (2020).
38. Hickey, B. M. S. L., Geier, S., Kachel, N. & MacFadyen, A. A bi-directional river plume: the Columbia in summer. *Continental Shelf Res.* **25**, 1631–1656 (2005).
39. Livneh, B. et al. A long-term hydrologically based dataset of land surface fluxes and states for the conterminous United States: update and extensions. *J. Clim.* **26**, 9384–9392 (2013).
40. Chapman, W. E. et al. Monthly modulations of ENSO teleconnections: implications for potential predictability in North America. *J. Clim.* **34**, 5899–5921 (2021).
41. Liu, Y. C., Di, P., Chen, S. H. & DaMassa, J. Relationships of rainy season precipitation and temperature to climate indices in California: long-term variability and extreme events. *J. Clim.* **31**, 1921–1942 (2018).
42. Mo, K. C. & Livezey, R. E. Tropical-extratropical geopotential height teleconnections during the Northern Hemisphere winter. *Mon. Wea. Rev.* **114**, 2488–2515 (1986).
43. Barnston, A. G. & Livezey, R. E. Classification, seasonality and persistence of low-frequency atmospheric circulation patterns. *Mon. Wea. Rev.* **115**, 1083–1126 (1987).
44. Li, A. K., Paek, H. & Yu, J. Y. The changing influences of the AMO and PDO on the decadal variation of the Santa Ana winds. *Environ. Res. Lett.* **11**, 064019 (2016).
45. Raphael, M. & Mills, G. The role of mid-latitude Pacific cyclones in the winter precipitation of California. *Prof. Geogr.* **48**, 251–262 (1996).
46. Gershunov, A., Shulgina, T., Ralph, F. M., Lavers, D. A. & Rutz, J. J. Assessing the climate-scale variability of atmospheric rivers affecting western North America. *Geophys. Res. Lett.* **44**, 7900–7908 (2017).
47. IPCC, 2022: *Climate Change 2022: Impacts, Adaptation, and Vulnerability*. Contribution of Working Group II to the Sixth Assessment Report of the Intergovernmental Panel on Climate Change (eds Pörtner, H.-O. et al.). Cambridge Univ. Press, in the press.
48. Ralph, F. M. et al. A scale to characterize the strength and impacts of atmospheric rivers. *Bull. Am. Meteorol. Soc.* **100**, 269–289 (2019).
49. Rayner, N. A. et al. Global analyses of sea surface temperature, sea ice, and night marine air temperature since the late nineteenth century. *J. Geophys. Res.* **108**, 4407 (2003).
50. Huang, B. et al. Extended reconstructed sea surface temperature, version 5 (ERSSTv5): upgrades, validations, and intercomparisons. *J. Clim.* **30**, 8179–8205 (2017).
51. Oppenheim, A. V., Schafer, R. W. & Buck, J. R. *Discrete-time signal processing*. Prentice Hall, 468–471 (1999).
52. Kalnay, E. et al. The NCEP/NCAR 40-year reanalysis project. *Bull. Am. Meteorol. Soc.* **77**, 437–470 (1996).
53. Muller, C. J., Back, L. E., O'Gorman, P. A. & Emanuel, K. A. A model for the relationship between tropical precipitation and column water vapor. *Geophys. Res. Lett.* **36**, L16804 (2009).
54. Crameri, F. Scientific colour maps: perceptually uniform and colour-vision deficiency friendly. *Zenodo*, <https://doi.org/10.5281/zenodo.1243862> (2018).

## Acknowledgements

This study was funded in part by the U.S. Army Corps of Engineers (W912HZ1920020) and the California Department of Parks and Recreation, Natural Resources Division Oceanography Program (C19E0026). Additional co-author support in part from NSF OCE-1924005. The Shore Stations Program is currently funded by the California Department of Parks and Recreation, Natural Resources Division, Award #C1670003. We thank all collectors who contributed to the Shore Stations datasets. Data were collected by Shore Station staff and volunteers starting March 2020 to present. From 1950 to 2020 data were collected by aquarists and volunteers with the Birch Aquarium at SIO. Prior to 1950, data were collected by Scripps staff and tide observers.

## Author contributions

S.M.B. led the data analysis and writing. M.A.M. contributed to and guided the analysis and writing. S.N.G., A.G., D.R.C., M.L.C., and R.E.F. provided analytical insight and feedback on the analysis and written content.

## Competing interests

The authors declare no competing interests.

## Additional information

**Supplementary information** The online version contains supplementary material available at <https://doi.org/10.1038/s43247-023-00803-8>.

**Correspondence** and requests for materials should be addressed to Sierra M. Byrne.

**Peer review information** *Communications Earth & Environment* thanks Jeannine-Marie St-Jacques and the other, anonymous, reviewer(s) for their contribution to the peer review of this work. Primary Handling Editors: Regina Rodrigues and Joe Aslin. Peer reviewer reports are available.

**Reprints and permission information** is available at <http://www.nature.com/reprints>

**Publisher's note** Springer Nature remains neutral with regard to jurisdictional claims in published maps and institutional affiliations.



**Open Access** This article is licensed under a Creative Commons Attribution 4.0 International License, which permits use, sharing, adaptation, distribution and reproduction in any medium or format, as long as you give appropriate credit to the original author(s) and the source, provide a link to the Creative Commons license, and indicate if changes were made. The images or other third party material in this article are included in the article's Creative Commons license, unless indicated otherwise in a credit line to the material. If material is not included in the article's Creative Commons license and your intended use is not permitted by statutory regulation or exceeds the permitted use, you will need to obtain permission directly from the copyright holder. To view a copy of this license, visit <http://creativecommons.org/licenses/by/4.0/>.

© The Author(s) 2023